# Highly Extensible Bio-Nanocomposite Fibers

Akhilesh K. Gaharwar, Patrick J. Schexnailder, Avinash Dundigalla, James D. White, Cristina R. Matos-Pérez, Joshua L. Cloud, Soenke Seifert, Jonathan J. Wilker, Gudrun Schmidt*

Here, we show that a poly(ethylene oxide) polymer can be physically cross-linked with silicate nanoparticles (Laponite) to yield highly extensible, bio-nanocomposite fibers that, upon pulling, stretch to extreme lengths and crystallize polymer chains. We find that both, nanometer structures and mechanical properties of the fibers respond to mechanical deformation by exhibiting strain-induced crystallization and high elongation. We explore the structural characteristics using X-ray scattering and the mechanical properties of the dried fibers made from hydrogels in order to determine feasibility for eventual biomedical use and to map out directions for further materials development.

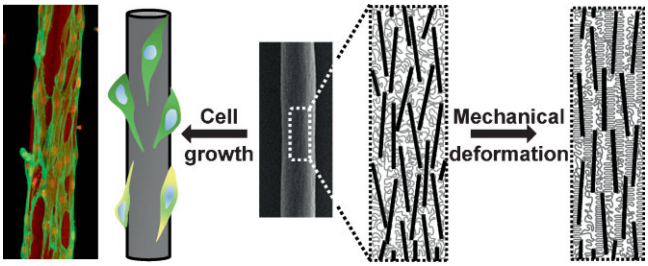


## Introduction

Nanocomposites made from a variety of synthetic or natural polymers and silicate nanoparticles have generated much attention in polymer science and many of the related interdisciplinary fields.[1–5] Mostly used for mechanical reinforcement, but also barrier and membrane separation properties, the flame resistance, ion conductivity, electro-optical, as well as other cosmetic, pharmaceutical, and biotechnological property enhancements suggest use for these materials in a broad spectrum of applications.[6–9] We are particularly interested in developing polymer nanocomposites for orthopedic surgery as the composition of some synthetic layered silicates and their dissolution products are similar to those of bioactive glasses used in bone repair.[10–12]

To formulate polymer nanocomposites and tailor the material properties toward a specific function, a fundamental understanding and knowledge of the nanometer structures and molecular interactions is necessary.[13–16] Well known model systems for studying polymer nanoparticle interactions and shear-orientations include nanocomposite gels from poly(ethylene oxide) (PEO) and Laponite nanoparticles.[17–20] These polymer nanocomposite materials have defined structures and mechanical properties that are a result of charged silicate nanoparticles acting as physical cross-linkers to the PEO.[2,21–23] In aqueous solutions the polymer readily adsorbs onto the nanoparticle surfaces and forms a reversible and physically cross-linked network. However, fiber morphologies made from this system have not been studied in detail.[24]

In this contribution, we present nanometer structures and mechanical properties of nanocomposite hydrogel fibers that in a dried state respond to mechanical deformation by exhibiting strain-induced crystallization.

G. Schmidt, A. K. Gaharwar, P. J. Schexnailder
Weldon School of Biomedical Engineering, Purdue University, West Lafayette, Indiana 47907, USA
Fax: +1 765 496 1912; E-mail: gudrun@purdue.edu
A. Dundigalla
Department of Chemistry, Louisiana State University, Baton Rouge, Louisiana 70803, USA
J. D. White, C. R. Matos-Pérez, J. L. Cloud, J. J. Wilker
Department of Chemistry, Purdue University, West Lafayette, Indiana 47907, USA
S. Seifert
Chemistry Division, Argonne National Laboratory, Argonne, Illinois 60439, USA




DOI: 10.1002/marc.201000556

Although neither the PEO polymer nor the silicate nanoparticles, alone, can support cell adhesion and growth, we show that this combination generates a synergy used by fibroblast cells to attach and align themselves along the fiber axes.

## Experimental Part

Poly(ethylene oxide) (PEO) with a molecular weight ($\overline{M}_w$) of $10^6$ g · mol$^{-1}$ and a weight-average molecular mass distribution of 1.5 was purchased from Polysciences Inc. Laponite RD (LRD), $Na^+_{0.7}[(Mg_{5.5}Li_{0.3})Si_8O_{20}(OH)_4]^-_{0.7}$, from Southern Clay Products Inc., is a synthetic Hectorite-type silicate clay consisting of nanoplatelets with an average diameter of 25–30 nm and a thickness of ≈1 nm. Laponite cross-linked PEOs were prepared from hydrogels composed of 2 wt.-% PEO and 3 wt.-% LRD via a gel/solvent exfoliation method.[22] Fibers were drawn manually and then dried at 25 °C in desicators and under vacuum for a week. The composition of fibers after solvent evaporation was ca. 60% LRD and 40% PEO (by mass fraction). The solution pH and ionic strength in the hydrogel were held constant by adding $10^{-4}$ M NaOH and $10^{-3}$ M NaCl, respectively.

Fibers were pulled from hydrogels and dried under vacuum for 2–3 d before imaging. A reproducible fiber diameter with less than 9% relative error can be achieved when the same pulling procedures are used. Polarized microscopy was done using an Olympus BX51 microscope (Olympus, Melville, NY, USA) with the application of a first order wavelength gypsum plate. For electron microscopy, fibers were sputter-coated with gold and palladium using an Edwards S-150 sputter coater. Scanning

Scanning electron microscopy (SEM) was performed with a Cambridge 260 Stereoscan Electron Microscope. Representative images are shown.

Mechanical testing was done using an Instron 5544 materials testing system and an LE3-2 system from Test Resources Inc. Linear variable differential transformer (LVDT) output was used to control the actuator at 25 °C. Grip regions were reinforced with paper to eliminate the possibility of failure at grips. Mechanical tests of the "starting fibers" were performed after the freshly prepared samples were dried at 25 °C in desiccators and under vacuum for one week. For mechanical testing of "prestretched fibers," first the starting fibers were stretched at 10 mm · min$^{-1}$ till failure and then the stretched sections were immediately subjected to subsequent mechanical testing at different stain rates. Reproducible mechanical testing data were obtained when measurements were repeated with new samples (ca. % relative error).

Small-angle X-ray scattering (SAXS) and wide-angle X-ray scattering (WAXS) measurements were performed at Argonne National Laboratory (Advanced Photon Source) using the undulator beamline 12ID-C (11 keV). A momentum transfer ($q$) of $0.025 < q < 0.6$ Å$^{-1}$ for SAXS and $0.4 < q < 2.4$ for WAXS was used. The scattering vector, $q$, was calibrated using a silver behenate standard at $q = 1.076$ Å$^{-1}$. The 2-D SAXS scattering images were corrected for spatial distortion and sensitivity of the detector and then radially averaged to produce scattered intensity, $I(q)$, versus $q$, where $q = (4\pi/\lambda)\sin\theta$.

NIH 3T3 mouse fibroblast cells (purchased from the American Type Culture Collection) were grown in Dulbecco's Modified Eagle's Medium supplemented with 10% bovine calf serum, 100 U · mL$^{-1}$ penicillin, 100 μg · mL$^{-1}$ streptomycin, and $4 \times 10^{-3}$ M L-glutamine. Fibers were briefly submersed in 70% ethyl alcohol and allowed to dry under sterile conditions. Fibers and control wells were seeded at 7 500 cells · cm$^{-2}$. Media was changed every third day. Cell number was quantified by measuring the absorbance at 490 nm using the CellTiter96 Aqueous One Solution Cell Proliferation Assay (Promega) as the metabolic indicator. For confocal imaging, fibers were seeded at 100 000 cells · cm$^{-2}$. Cells were fixed using 3.7% formaldehyde solution after 3 h and 7 d. The cytoskeleton of cells was labeled with Alexa Fluor 488 phalloidin, and the nuclei were counterstained with 7-aminoactinomycin D (7-AAD, Invitrogen). Fluorescent images were taken with an Olympus FV1000 confocal microscope with an excitation wavelength of 488 nm for Alexa-Fluor488 and 543 nm for 7-AAD. Representative images are shown.

## Results and Discussion

We use Laponite silicate nanoplatelets to physically cross-link PEO and generate a nanocomposite hydrogel that can be pulled to form fibers. Upon stretching, flexibility, and extreme elongation are found and the fibers dry during stretching. When pulled we observe greater alignment of the nanoplatelets within fibers and crystallization of polymer chains. The material provides a substrate for fibroblast growth, with cells observed surrounding the fibers and aligning along the fiber axis. This cell adhesion and alignment is especially exciting given that neither the polymer, alone, nor the nanoplatelets, alone, can harbor cells in this manner.

### Surface Morphology of Nanocomposite Fibers

Figure 1a shows a hydrogel formulation from which a gel fiber can be drawn manually. At this composition (3 wt.-% LRD and 2 wt.-% PEO) an individual gel fiber may be drawn up to 5 m long. We refer to this gel–fiber formation as starting fibers. As the fiber is drawn, its diameter is reduced, the solvent evaporates, the polymer and nanoparticle cross-linkers are aligned, and the fiber appears birefringent under crossed polarizers (Figure 1b–d). Birefringence usually originates from the orientation of anisotropic structures such as elongated polymer chains, from oriented or crystallized polymer domains or from aligned nanoparticles. Our observations show that birefringence disappears when the fibers are heated above the polymer melting temperature (PEO ≈60 °C). This observation suggests that the birefringence must be dominated by polymer orientation rather than by silicate nanoparticle orientation.

SEM images of dried nanocomposite fibers show a relatively smooth surface morphology (Figure 1e and f). When semi-wet fibers are repeatedly stretched and relaxed during the drying process, coiled, instead of straight, fibers can be formed (Figure 1g and h). We assume that hydrogen

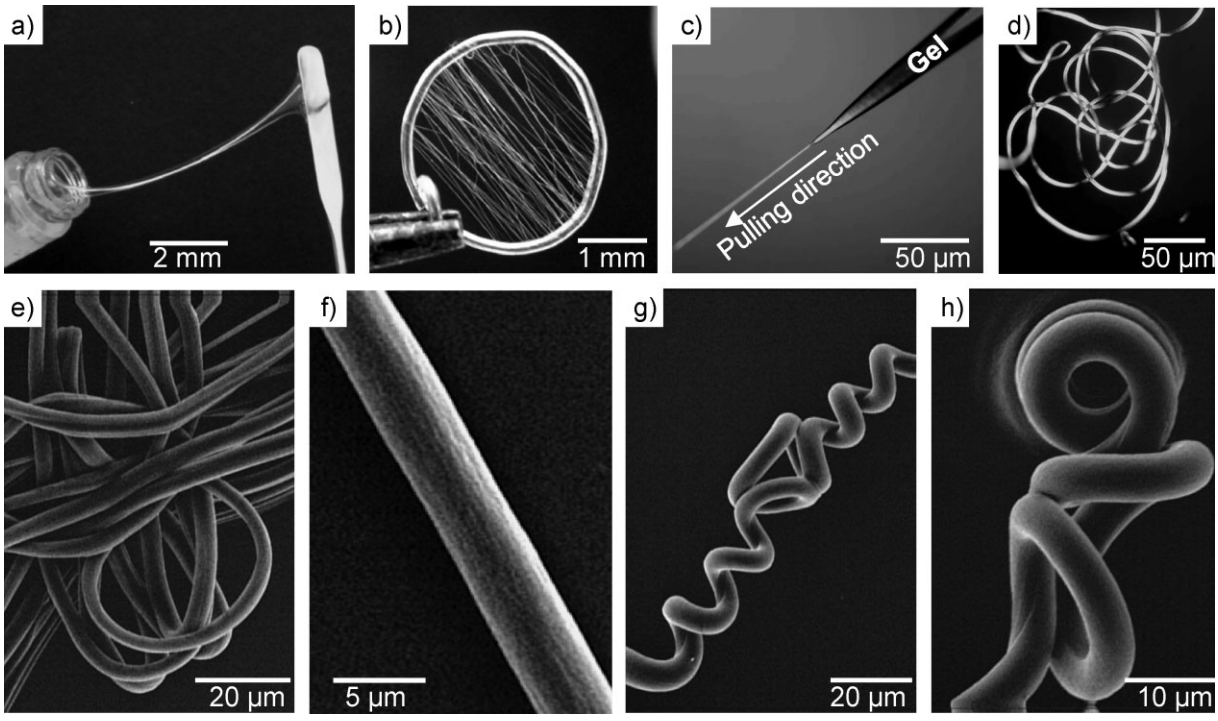


*Figure 1.* Nanocomposite fibers made from hydrogels. (a) Nanoplatelet cross-linking of PEO yields a viscous hydrogel that can be pulled into hydrogel fibers over 5 m long, which dry when exposed to air. (b) Semi-dried fibers wrapped around a metal loop. Fibers dry when exposed to air. (c) Birefringent hydrogel fiber pulled from the hydrogel seen under cross-polarized light. (d) Cross-polarized image of a birefringent semi-dried fiber suggesting anisotropic orientation. The diameter of manually drawn gel fibers depends upon the drawing ratio and varies between 1 and 100 μm. (e) SEM image of intertwined and (f) straight fibers. (g) and (h) Fibers with helical structures obtained after stretching and breaking. All fibers have smooth surface morphology and high aspect ratios.

bonding combined with strong ionic interactions must be responsible for the unique elongational properties.

### Unique Elongational Properties of Fibers as Tested by Mechanical Deformation

Figure 2a and b show typical stress–strain curves for fibers drawn from the hydrogel and then dried. We will refer to the initial testing of dried fibers as starting fibers and to the testing of prestretched fibers for fibers which were stretched at $10\,mm \cdot min^{-1}$ (till failure) prior to data collection. Mechanical testing and qualitative visual observations indicate that the deformation of fibers results in necking. The neck region becomes more pronounced with deformation, and the fiber becomes more birefringent. Before deformation, the fiber is transparent to eye but becomes opaque with deformation. The fibers display a sharp conventional yield point, and the stepwise deformation behavior in the form of serration on stress–strain curves is similar to what is observed for other polymers.[25] A neck forms at early stages of the deformation (less than 5% strain) immediately after the yield, and a high degree of birefringence is observed in the neck region under polarized light. The plastic strain in the fiber may be generated by several different molecular processes such as chain slip, chain tilt, and lamellar break-up. The neck propagates along the length of the fiber (similar to cold drawing), resulting in a deformed fiber of uniform length. The ductile fracture mode can be characterized by formation of a cup and cone at the instability junction.

Mechanical properties are summarized in Figure 2c. The impact of strain rate on the modulus, yield stress, and total strain is significant. A two-fold increase in modulus, yield stress, and failure stress is observed when the strain rate goes from 10 to $50\,mm \cdot min^{-1}$, while the total strain increases four-fold (≈950%). The elongation of the starting fibers is higher when higher strain rates are applied. This behavior is particularly interesting because polymers usually extend less at greater loading rates. Maximum elongation is ca 950% (ca. 1 m long) before the dried fiber breaks. For comparison, a fiber pulled from the starting gel could be elongated up to 5 m, thus drying significantly reduces the elongational capabilities.

The high amount of silicate nanoparticles (60 wt.-%) in the nanocomposite fibers might be responsible for the unique properties combinations. The high stain rates result in alignment of polymer chains (that are reversibly cross-linked between silicate nanoparticles) along the stretching

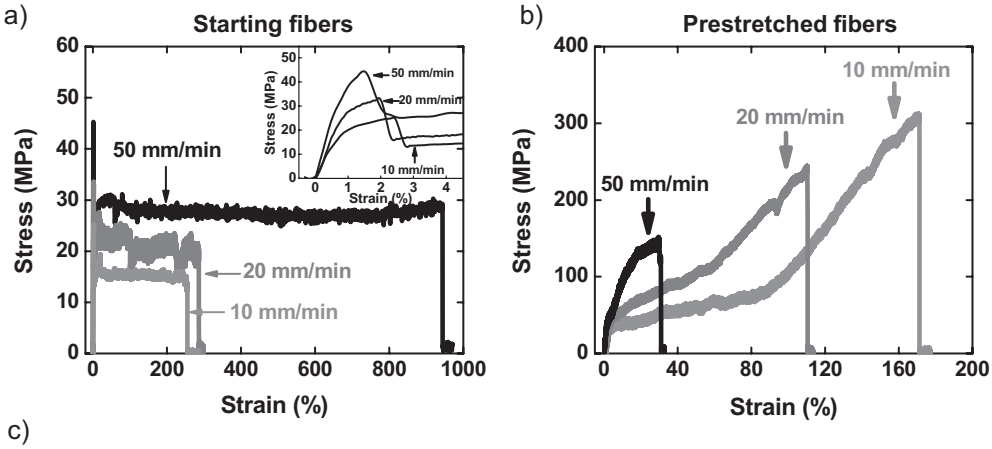


c)

| Sample | Strain rate | Modulus (MPa) | Yield strength (MPa) | Failure stress (MPa) | Ultimate strain (%) |
|---|---|---|---|---|---|
| Starting fibers | 10 mm/min | 16 ± 2 | 24 ± 3 | 15 ± 1 | 250 ± 10 |
| | 20 mm/min | 20 ± 2 | 33 ± 3 | 21 ± 1 | 280 ± 18 |
| | 50 mm/min | 29 ± 2 | 45 ± 5 | 30 ± 2 | 950 ± 29 |
| Prestretched fibers | 10 mm/min | 14 ± 1 | -- | 315 ± 24 | 170 ± 22 |
| | 20 mm/min | 18 ± 1 | -- | 245 ± 13 | 115 ± 19 |
| | 50 mm/min | 27 ± 2 | -- | 160 ± 5 | 30 ± 6 |

*Figure 2.* Mechanical properties of nanocomposite fibers. (a) Typical stress–strain curves of thick fibers (≈75–100 μm) at different strain rates (10, 20, and 50 mm · min$^{-1}$). Starting fibers were drawn from the hydrogel and then dried. The inset shows the initial region of the stress–strain curves. The elastic modulus and yield stress increases with increase in strain rate. (b) Stress–strain curves for the "prestretched fibers" at different strain rates. (c) Mechanical properties of starting fibers and prestretched fibers are summarized. Reported values are means ± s.d. ($n = 5$). Modulus increases with increasing strain rate for both starting and prestretched fibers. Ultimate elongation also increases with increasing strain rate for starting fibers, but decreases for prestretched fibers. Failure stress slightly increases with increasing strain rate for starting fibers, but significantly decreases for prestretched fibers.

direction. As a result highly ordered, lamellar or fibrillar domains are formed. These domains facilitate the further pulling of silicate nanoparticles from the unstretched nanocomposite network which leads to highly aligned structures on all length scales.

Additional drawing of the pre-stretched fibers can enhance the mechanical strength of the nanocomposite fibers. This procedure is very similar to the dry spinning process that is applied to enhance the mechanical properties of already oriented films and fibers.[26] Such materials then undergo additional deformation while remaining cohesive enough to support the stresses during elongation. Stress–strain curves for the fibers obtained after prestretching are shown in Figure 2b. Strain hardening and shorter elongations-to-fail were observed relative to the starting, unstressed fibers. Stress values obtained for prestretched fibers were ca. 10 times that of the starting fibers. Typical combinations of silicate and elastomeric polymers[3,5,27] tend to be either stiff but not extensible or extensible but not stiff. Here, we show that silicate cross-linked nanocomposite fibers (starting fibers) are highly extensible, in a dried state by nearly 1 000%. After pre-stretching, the fibers are less extensible but display an increased failure stress (by ca. 10×). These unique mechanical properties are mainly a result of physical interactions between the charged Laponite nanoparticles and PEO chains. In addition to hydrogen bonding to residue water molecules, interactions are of ionic nature as the charges of the Laponite may interact with the PEO polymer chains. The coordination between the PEO chains and the alkali metal ions present on the surface of silicate nanoparticles will lead to additional reinforcement of the network structures.

Several studies from literature proposed PEO-silicate-salt structures and orientations in which cations are residing at the surface of the silicate nanoparticles.[28,29] Other studies proposed architectures that involve helical PEO structures in which the cation resides within the center of the polymer helix and is coordinated with oxygen atoms from the PEO chains.[29,30]

## Nanometer Structural Orientation of Fibers as Tested by X-ray Scattering

In order to characterize the polymer-nanoplatelet hierarchy within these fibers, scattering techniques, such as SAXS, provide structural information at the nanometer scale. A

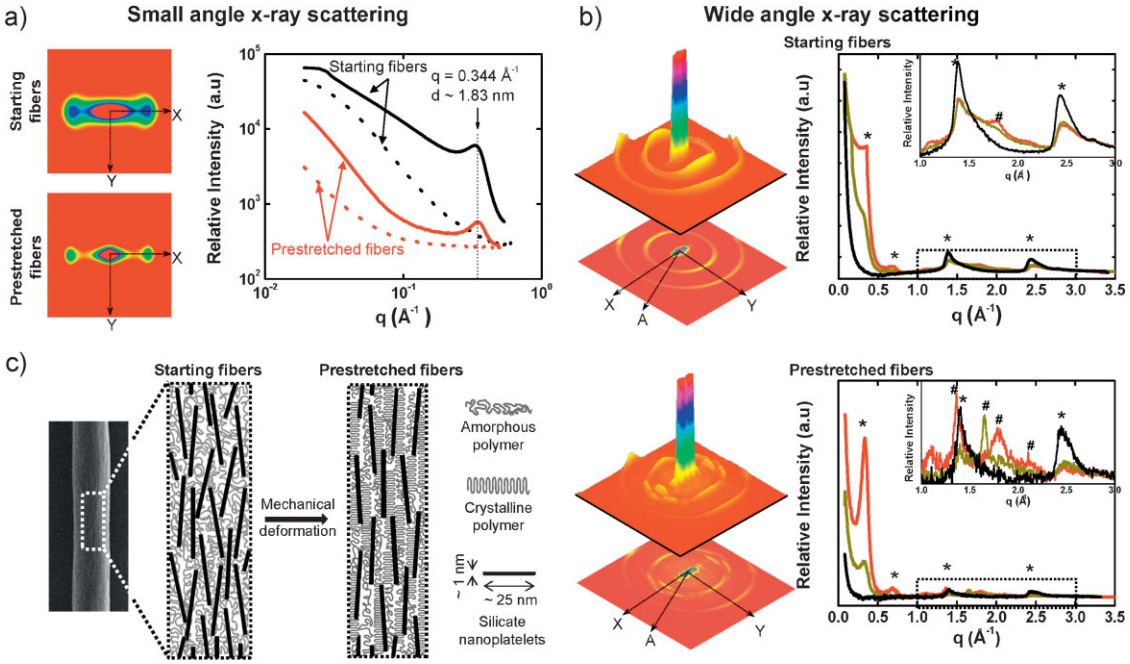


*Figure 3.* Small-angle X-ray scattering (SAXS) and WAXS techniques indicate alignment of nanostructures. (a) 2D SAXS spectra of starting fiber and prestretched fiber. Starting fibers showing a "dumbbell" shape. The presence of a streak along the equatorial plane indicates partially aligned polymer chains, whereas the symmetric pattern indicates lamellar nanostructures. Stretched fibers exhibit an SAXS pattern with the scattering maxima in the equatorial direction indicating formation of lamellar structures along the fiber axis. The observation of a sharp streak near the beam stop indicates the presence of highly oriented polymer chains. (a) right, Intensity as function of $q$ calculated from 2D SAXS patterns in X (solid) and Y (dotted) directions. Starting (black) and prestretched fibers (red) show an intercalated peak at $q = 0.344$ (Å$^{-1}$) which corresponds to a characteristic dimension $d = 2\pi/q = 1.83$ nm. Anisotropy is characterized by the intensity difference between X (solid) and Y (dotted) directions. Stretching causes increased SAXS anisotropy in the low $q$ region which corresponds to increased orientation of large scale domains (few 100 nm). (b) 3D and 2D WAXS spectra from a starting fiber and prestretched fiber. Intensities as function of momentum transfer, $q$, calculated from 2D WAXS pattern in different direction [X (red)-, Y(black),- and A(green)]. The four prominent peaks (X- and A-) in starting fibers correspond to (001), (002), (003), and (004) Laponite planes (indicated by asterisk). 3D and 2D WAXS pattern of prestretched fiber indicates formation and alignment of PEO crystallite. The 2D WAXS pattern shows eight characteristic arcs that can be correlated to the monoclinic crystal structure of PEO. Intensities as function of momentum transfer, $q$, calculated from 2D WAXS pattern in X (red) and A (green) direction show presence of PEO peaks (indicated by hatch). These data show that PEO chains crystallized due to serve mechanical deformation and these crystallite domains get aligned along the fiber axis. (c) Representation of Laponite nanoplatelets and PEO polymer chains in the fiber before and after stretching. Prior to deformation, the nanoplatelets are aligned along the fiber axis and the polymer is predominantly amorphous. Mechanical deformation provides orientation of polymer chains and strain-induced crystallization of the confined polymer (highly oriented polymer crystallites).

fully exfoliated nanocomposite does not show diffraction peaks due to very large distances or random orientations between the silicate platelets, while an intercalated nanocomposite with well defined spatial relationship between polymer chains and nanoplatelets shows a diffraction peak corresponding to the inter-layer distance. In addition to these two well-defined structures, other intermediate structures can be obtained.

Results presented in Figure 3, show SAXS and WAXS spectra and averaged scattering intensities versus momentum transfer, $q$ from a starting fiber and from a prestretched fiber. Figure 3a, top left, shows a 2D SAXS scattering pattern for the starting fibers in which a "dumbbell" shape and a weak equatorial plane streak can be seen. This plot indicates that the starting fibers exhibit a degree of nanoscale orientation, where the presence of the weak equatorial plane streak indicates aligned polymer chains and the symmetric bell pattern indicates the presence of deformed lamellar structures. The prestretched fibers, by contrast (Figure 3a, bottom left), display an SAXS trace with more pronounced scattering maxima at the equatorial extremes. The prestretched fiber exhibits "lobe" patterns, indicating transformation of lamellar structure to fibrillar structure.[31] These data indicate that mechanical force introduces a marked alignment of polymer chains and stacked silicate platelets coincident with the fiber axis.

The degree of anisotropy in the fibers can be estimated from the extent of bifurcation in X- and Z-intensity at low $q$ (Figure 3a, right). A maximum in intensity observed at high $q$ ($q = 0.344$ Å$^{-1}$) corresponds to a characteristic length ≈1.83 nm which is a result of fiber drawing. This 1.83 nm distance is related to the 001 basal plane spacing between

PEO covered Laponite platelets. The scattering maximum is more pronounced when a fiber is prestretched. A pure Laponite film consisting of layered platelets, has an average distance between platelets of ca. 1.34 nm.[32] The increase in interlayer distance between pure Laponite films and PEO covered Laponite fibers is ≈0.49 nm, and corresponds to the adsorbed and intercalated polymer.

Interrogation of the starting fibers by WAXS methods showed peaks attributable to the polymer intercalated Laponite 001 ($q = 0.345$ Å$^{-1}$, 1.83 nm), 002 ($q = 0.688$ Å$^{-1}$, 0.91 nm), 003 ($q = 1.394$ Å$^{-1}$, 0.45 nm), and 004 ($q = 2.440$ Å$^{-1}$, 0.25 nm) planes (Figure 3b, top). Drawing the fibers presented the same features as starting fibers along with the introduction of several new peaks (Figure 3b, bottom). In addition to providing information on the Laponite orientation, WAXS was also used to evaluate polymer crystallinity. Apart from (00L) peaks, we observed new peaks in prestretched fibers. The diffraction patterns from prestretched fibers indicate the presence of PEO crystallites oriented along the stretching direction. These diffraction patterns show eight characteristic arcs that can be correlated to the monoclinic crystal structure of PEO ($a = 8.05$ Å, $b = 13.04$ Å, $c = 19.84$ Å, $\beta = 125.4^{\circ}$).[33,34] The two equatorial peaks perpendicular to the stretching direction indicate the (120) crystallographic planes ($q \approx 1.36$ Å$^{-1}$) and the four peaks in the quadrants correspond to the (112) crystallographic planes ($q \approx 1.65$ Å$^{-1}$). The appearance of PEO crystallographic peaks after stretching indicates that mechanical deformation results in alignment and crystallization of PEO chains along the stretching direction. These data show that strain-induced crystallization of the PEO chains aligns these crystallite domains along the fiber axis. The WAXS patterns display significant horizontal intensities before and after stretching (Figure 3b) and provide further support for confined PEO crystallization[33] and orientation[34] along the fiber axis when placed under strain.

Optically, these fibers appeared transparent prior to stretching but became opaque under strain. Examination by polarizing microscopy showed a gain in birefringence upon pulling, further indicating microscopic orientation along the fiber axis (Figure 1c). Along with the SAXS and WAXS plots, these data provide a picture in which the starting fibers exhibit a limited initial degree of polymer chain orientation and lamellar structure. The interaction of PEO with Laponite leaves the PEO amorphous within the hydrogel. From our experience with PEO–Laponite films, shearing and rapid solvent evaporation result in the formation of ordered structures and the polymer covered silicate platelets orient along the shear direction (fiber axis).[2] Upon further stretching, the polymer chains and nanoplatelets become further oriented along the tensile direction and crystallize (Figure 3c). The crystallites orient parallel to the tensile direction, and the fiber takes on a more ordered, lamellar or fibrillar nanostructure. This hypothesis is supported by the results obtained from mechanical analysis, optical microscopy, and X-ray scattering and may explain how these fibers can be stretched to such lengths and subsequent increase in tensile strength.

### Cell Alignment Along the Fiber Axis

The ability to dictate material structure by synergistic combination of properties, is key to the development of new biomaterials.[9,35,36] Equally important is the ability of cells to attach onto such a material. Starting fibers as well as stretched fibers were incubated in media with NIH 3T3 fibroblasts and stained to visualize the actin cytoskeleton. Figure 4a–d shows confocal micrographs indicating that the cells not only grow on the fibers but adapt to the surface morphology, encapsulate some of the fibrous structure, and align actin filaments along the fiber axes. Neither PEO[37] nor Laponite, alone, are capable of supporting any such cell attachment and alignment. Consequently this polymer-silicate nanoplatelet combination exhibits a synergy with regard to cell adhesion and proliferation. Moreover, the morphology of cells on nanocomposite fibers is different when compared to TCPS and nanocomposite films (inset in Figure 4e). The cytoskeleton alignment of cells seeded on nanocomposite fibers can be attributed to the alignment of the silicate nanoparticles. To our knowledge there is no literature on PEO-silicate fibers that induce such cell alignment. However, recent studies on self-assembled supramolecular peptide filaments showed similar kind of cell alignment within hydrogel fibers.[38] Other polymeric fibers that have been used for cell alignment were made e.g., from poly(L-lactic acid),[39] poly[lactic-*co*-(glycolic acid)),[40] and poly(ethylene terephthalate).[39]

Significant proliferation was found with a 2D film made from the same composition of PEO cross-linked with the silicate suggesting that the material is promising for further biomaterials development (Figure 4e). The number of cells on TCPS at the plateau phase of the cell growth curve is significantly higher compared to the nanocomposites. In our previous studies we have shown that the cell numbers reached in the plateau phase of the cell growth curves were not a result of contact inhibition between cells.[2,11,41] Instead, growth inhibition was found to be dependent on the number and distribution of "cell repellant" PEO and "cell adhesive" silicate regions on the nanocomposite films.[2,11,41] Similar effects are found in the cell growth experiments on fiber surfaces showing that cells are not confluent (Figure 4).

Finally, prolonged submersion of fibers in aqueous solution leads to fiber swelling and diminishes some of the noted extensibility but does not affect cell adhesion. Thus knowledge of the nanometer structures and polymer nanoparticle interactions is necessary to better understand

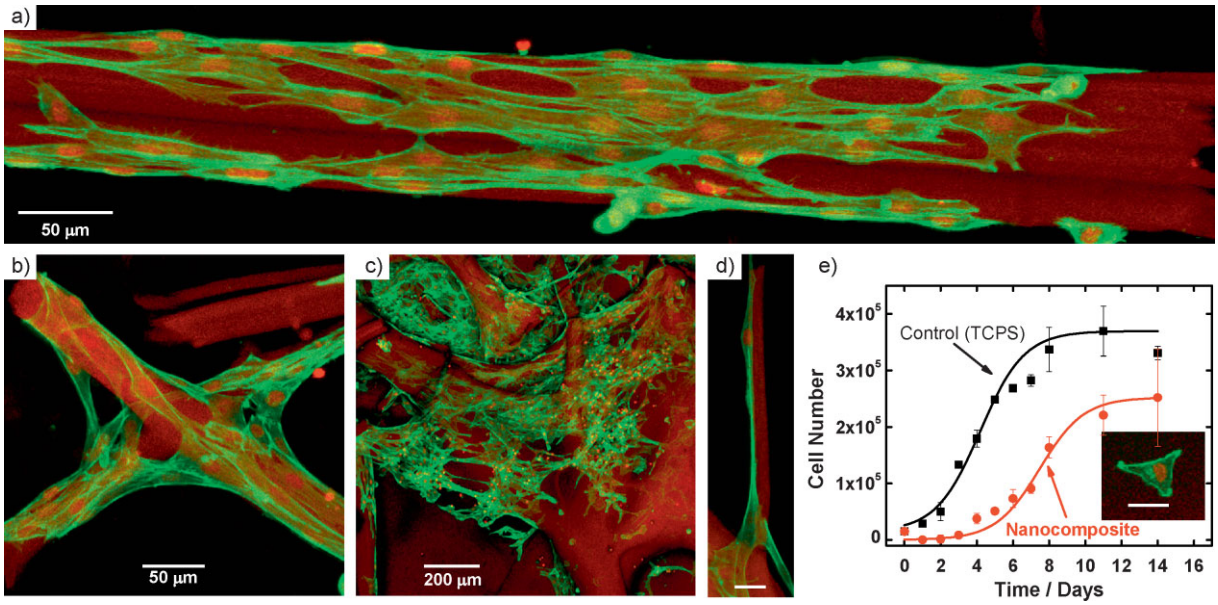


*Figure 4.* NIH 3T3 fibroblasts grow on top of and around nanocomposite fibers. 2D confocal microscopy images were generated from 3D stack images. Cells were stained with phalloidin to visualize the F-actin cytoskeleton network. (a) and (b) Images showing that fibroblasts grow on the fibers, can encapsulate the surface and adapt to the surface morphology. These images show uniform distribution of cells over the fibers. Note that F-actin cytoskeleton filaments tend to align along the fiber axis, especially visible in frame a. Thick fibers have been used here to better show cell growth. (d) The cytoskeleton of cells seeded on nanocomposite fibers show alignment of the actin filaments along the fiber axis, whereas no specific alignment was observed when cells were seeded on TCPS control or 2D nanocomposite films (inset in Figure 4e). Scale bar represent 25 μm. (e) Growth curves of NIH 3T3 fibroblasts on nanoplatelet cross-linked polymer films and a tissue culture polystyrene (TCPS) control. Plotted values are means ± s.d. ($n = 3$).

the material properties for future improvement of properties. Our results suggest that further development of these nanocomposite fiber materials might be useful for a broad spectrum of biomedical applications where cell adhesion can be controlled.

## Conclusion

Taken together, data presented here show that silicate nanoplatelets can induce polymer cross-linking strong enough to yield fiber materials with intriguing mechanical properties. The fibers display extreme elongation and can be drawn to high aspect ratios. Upon deformation, polymer chains within the starting fibers crystallize and, along with the nanoplatelets, orient parallel to the fiber axis. Although PEO cannot support cell growth, the silicate cross-linked nanocomposite fibers provides a suitable substrate for fibroblast adhesion and guided cell growth.

Acknowledgements: This research has been supported in part by a *National Science Foundation Career award* (GS) and the *Office of Naval Research* (JJW).

Received: August 28, 2010; Revised: October 20, 2010; Published online: December 3, 2010; DOI: 10.1002/marc.201000556

Keywords: bio-nanocomposites; fibers; mechanical properties; poly(ethylene oxide); silicates

[1] L. J. Bonderer, A. R. Studart, L. J. Gauckler, *Science* **2008**, *319*, 1069.
[2] A. K. Gaharwar, P. Schexnailder, V. Kaul, O. Akkus, D. Zakharov, S. Seifert, G. Schmidt, *Adv. Funct. Mater.* **2010**, *20*, 429.
[3] S. M. Liff, N. Kumar, G. H. McKinley, *Nat. Mater.* **2007**, *6*, 76.
[4] G. Mayer, *Science* **2005**, *310*, 1144.
[5] P. Podsiadlo, A. K. Kaushik, E. M. Arruda, A. M. Waas, B. S. Shim, J. Xu, H. Nandivada, B. G. Pumplin, J. Lahann, A. Ramamoorthy, N. A. Kotov, *Science* **2007**, *318*, 80.
[6] D. R. Paul, L. M. Robeson, *Polymer* **2008**, *49*, 3187.
[7] C. J. Wu, A. K. Gaharwar, P. J. Schexnailder, G. Schmidt, *Materials* **2010**, *3*, 2985.
[8] R. A. Vaia, J. F. Maguire, *Chem. Mater.* **2007**, *19*, 2736.
[9] P. Schexnailder, G. Schmidt, *Colloid Polym. Sci.* **2009**, *287*, 1.
[10] L. L. Hench, I. D. Xynos, J. M. Polak, *J. Biomater. Sci., Polym. Ed.* **2004**, *15*, 543.
[11] A. K. Gaharwar, P. J. Schexnailder, B. Kline, G. Schmidt, *Acta Biomater.* **2010**, DOI: 10.1016/j.actbio.2010.09.015.
[12] A. K. Gaharwar, P. J. Schexnailder, Q. Jin, C.-J. Wu, G. Schmidt, *ACS Appl. Mater. Interfaces* **2010**, DOI: 10.1021/am100609t.
[13] M. Alexandre, P. Dubois, *Mater. Sci. Eng. R* **2000**, *28*, 1.
[14] E. P. Giannelis, *Adv. Mater.* **1996**, *8*, 29.

[15] P. C. LeBaron, Z. Wang, T. J. Pinnavaia, *Appl. Clay Sci.* **1999**, *15*, 11.
[16] S. Ray, *Prog. Mater. Sci.* **2005**, *50*, 962.
[17] H. A. Baghdadi, H. Sardinha, S. R. Bhatia, *J. Polym. Sci. Polym. Phys.* **2005**, *43*, 233.
[18] E. Loizou, L. Porcar, P. Schexnailder, G. Schmidt, P. Butler, *Macromolecules* **2010**, *43*, 1041.
[19] D. C. Pozzo, L. M. Walker, *Colloids Surf., A* **2004**, *240*, 187.
[20] G. Schmidt, A. I. Nakatani, P. D. Butler, A. Karim, C. C. Han, *Macromolecules* **2000**, *33*, 7219.
[21] E. Loizou, P. Butler, L. Porcar, G. Schmidt, *Macromolecules* **2006**, *39*, 1614.
[22] E. Loizou, P. D. Butler, L. Porcar, Y. Talmon, E. Kesselman, G. Schmidt, *Macromolecules.* **2005**, *38*, 2047.
[23] K. Shikinaka, K. Aizawa, N. Fujii, Y. Osada, M. Tokita, J. Watanabe, K. Shigehara, *Langmuir* **2010**, *26*, 12493.
[24] V. K. Daga, M. E. Helgeson, N. J. Wagner, *J. Polym. Sci. Polym. Phys.* **2006**, *44*, 1608.
[25] M. Rubinstein, R. H. Colby, "*Polymer Physics*", Oxford University Press, New York 2004.
[26] J. W. Leenslag, A. J. Pennings, *Polymer* **1987**, *28*, 1695.
[27] K. Haraguchi, M. Ebato, T. Takehisa, *Adv. Mater.* **2006**, *18*, 2250.
[28] J. Bujdak, E. Hackett, E. P. Giannelis, *Chem. Mater.* **2000**, *12*, 2168.
[29] P. Schexnailder, E. Loizou, L. Porcar, P. Butler, G. Schmidt, *Phys. Chem. Chem. Phys.* **2009**, *11*, 2760.
[30] D. J. Harris, T. J. Bonagamba, K. Schmidt-Rohr, *Macromolecules* **1999**, *32*, 6718.
[31] D. Kawakami, B. S. Hsiao, C. Burger, S. Ran, C. Avila-Orta, I. Sics, T. Kikutani, K. I. Jacob, B. Chu, *Macromolecules* **2005**, *38*, 91.
[32] T. N. Blanton, D. Majumdar, S. M. Melpolder, *Adv. X-Ray Anal.* **2000**, *42*, 562.
[33] H. Wang, J. K. Keum, A. Hiltner, E. Baer, B. Freeman, A. Rozanski, A. Galeski, *Science* **2009**, *323*, 757.
[34] L. Zhu, S. Z. D. Cheng, B. H. Calhoun, Q. Ge, R. P. Quirk, E. L. Thomas, B. S. Hsiao, F. Yeh, B. Lotz, *J. Am. Chem. Soc.* **2000**, *122*, 5957.
[35] I. Galaev, B. Mattiasson, "*Smart Polymers: Applications in Biotechnology and Biomedicine*", 2nd edition, CRC Presss, Boca Raton 2008.
[36] M. Yoshida, R. Langer, A. Lendlein, J. Lahann, *Polym. Rev.* **2006**, *46*, 347.
[37] J. M. Harris, "*Poly(ethylene glycol) Chemistry: Biotechnical and Biomedical Applications*", Plenum Press, New York, London 1992.
[38] S. Zhang, M. A. Greenfield, A. Mata, L. C. Palmer, R. Bitton, J. R. Mantei, C. Aparicio, M. O. de la Cruz, S. I. Stupp, *Nat. Mater.* **2010**, *9*, 594.
[39] Q. Lu, A. Simionescu, N. Vyavahare, *Acta Biomater.* **2005**, *1*, 607.
[40] C. Hwang, Y. Park, J. Park, K. Lee, K. Sun, A. Khademhosseini, S. Lee, *Biomed. Microdevices* **2009**, *11*, 739.
[41] P. J. Schexnailder, A. K. Gaharwar, R. L. Bartlett Ii, B. L. Seal, G. Schmidt, *Macromol. Biosci.* **2010**, DOI: 10.1002/mabi.201000053.